Notes

In the mortality analysis in which patients who underwent transplantation were followed and the data were not censored, the hazard ratio was 0.51 (95% CI, 0.31 to 0.86), favoring pirfenidone. These findings are consistent with and corroborate the results of the prespecified analysis of all-cause mortality (hazard ratio, 0.52; 95% CI, 0.31 to 0.87).

Talmadge E. King, Jr., M.D.
University of California, San Francisco
San Francisco, CA
tking@medicine.ucsf.edu

Paul W. Noble, M.D.
Cedars–Sinai Medical Center
Los Angeles, CA

Williamson Z. Bradford, M.D., Ph.D.
InterMune
Brisbane, CA

Since publication of their article, the authors report no further potential conflict of interest.

1. Collard HR, Moore BB, Flaherty KR, et al. Acute exacerbations of idiopathic pulmonary fibrosis. Am J Respir Crit Care Med 2007;176:636-43.
2. Lachin JM. Worst-rank score analysis with informatively missing observations in clinical trials. Control Clin Trials 1999;20:408-22.
3. Finkelstein DM, Schoenfeld DA. Combining mortality and longitudinal measures in clinical trials. Stat Med 1999;18:1341-54.

DOI: 10.1056/NEJMc1407776

The Metabolic Syndrome and *DYRK1B*

TO THE EDITOR: Keramati et al. (May 15 issue)[1] found that the gain-of-function *DYRK1B* variants R102C and H90P were associated with the metabolic syndrome. These findings probably reveal one end of the phenotypic spectrum associated with *DYRK1B* variants. The L28P variant of *DYRK1B* is predicted to be "damaging,"[2] and we have postulated that it may be a loss-of-function variant with a protective effect against the metabolic syndrome.

We performed a phenomewide association study to examine phenotypes associated with the L28P variant of *DYRK1B* in a cohort of 7800 Geisinger MyCode Project participants for whom existing genotype data (obtained with the use of the Illumina HumanExome BeadChip) were available and linked to electronic medical record data. Phenotypes associated with cardiometabolic disease were identified with the use of previously validated phenomewide association study codes.[3] Our study revealed a significant protective effect of L28P (in 42 heterozygotes) against type 2 diabetes and a trend toward a protective effect against hypertension (Table 1). Two *DYRK1B* variants (G352A and P578S) that were predicted to be benign had no significant associations in the phenomewide association study.

Some *DYRK1B* variants are associated with autosomal dominant protective effects. Electronic medical records linked to existing genomic data sets can be used to rapidly identify population-level genotype–phenotype associations.

Table 1. **Association of Clinical Conditions with the L28P Variant of *DYRK1B*, as Determined by Means of a Phenomewide Association Study.**

Condition	Adjusted Odds Ratio (95% CI)	Adjusted P Value*
Diabetes mellitus	0.30 (0.12–0.71)	0.002
Essential hypertension	0.52 (0.24–1.10)	0.09
Disorders of lipid metabolism	0.68 (0.30–1.53)	0.36
Overweight and obesity	0.91 (0.36–2.29)	0.85
Hypertensive heart disease	1.32 (0.39–4.41)	0.66
Myocardial infarction	0.36 (0.05–2.66)	0.24
Pulmonary heart disease	1.71 (0.52–5.64)	0.41
Heart failure	1.59 (0.65–3.87)	0.32
Symptoms involving cardiovascular system	1.34 (0.46–3.95)	0.60

* P values were adjusted for age, sex, and study group. CI denotes confidence interval.

Tooraj Mirshahi, Ph.D.
Michael F. Murray, M.D.
David J. Carey, Ph.D.
Geisinger Clinic
Danville, PA
tmirshahi@geisinger.edu

No potential conflict of interest relevant to this letter was reported.

1. Keramati AR, Fathzadeh M, Go G-W, et al. A form of the metabolic syndrome associated with mutations in *DYRK1B*. N Engl J Med 2014;370:1909-19.

2. Adzhubei IA, Schmidt S, Peshkin L, et al. A method and server for predicting damaging missense mutations. Nat Methods 2010;7:248-9.
3. Denny JC, Bastarache L, Ritchie MD, et al. Systematic comparison of phenome-wide association study of electronic medical record data and genome-wide association study data. Nat Biotechnol 2013;31:1102-10.

DOI: 10.1056/NEJMc1408235

TO THE EDITOR: Keramati et al. detected *DYRK1B* mutations in families with the metabolic syndrome. The authors state that the clinical features of affected family members cannot be explained by neurohormonal activation (the plasma levels of the five tested hormones were all within the normal ranges). However, we note that the R102C mutation induces increased expression of peroxisome-proliferator–activated receptor γ (PPAR-γ) and PPAR-γ coactivator-1 (also known as PCG-1-α), which are associated with plasma levels of adipokines (e.g., adiponectin, leptin, resistin, and fibroblast growth factor 21 [FGF-21]) that play crucial roles in the metabolic syndrome.[1-4] Therefore, these plasma adipokines are presumably more directly relevant than the five tested hormones in this special form of the metabolic syndrome. To explain the clinical features associated with neurohormonal activation, we suggest that in future studies adipokines should be taken into account as plasma biomarkers for this form of the metabolic syndrome.

Jian-Li He, M.S.
Guo-Fen Qiao, M.D., Ph.D.
Bai-Yan Li, M.D., Ph.D.
Harbin Medical University
Harbin, China
baili@iupui.edu

No potential conflict of interest relevant to this letter was reported.

1. Estall JL, Ruas JL, Choi CS, et al. PGC-1alpha negatively regulates hepatic FGF21 expression by modulating the heme/Rev-Erb(alpha) axis. Proc Natl Acad Sci U S A 2009;106:22510-5.
2. Miles PD, Barak Y, He W, Evans RM, Olefsky JM. Improved insulin-sensitivity in mice heterozygous for PPAR-gamma deficiency. J Clin Invest 2000;105:287-92.
3. Steppan CM, Bailey ST, Bhat S, et al. The hormone resistin links obesity to diabetes. Nature 2001;409:307-12.
4. Yamauchi T, Kamon J, Waki H, et al. The fat-derived hormone adiponectin reverses insulin resistance associated with both lipoatrophy and obesity. Nat Med 2001;7:941-6.

DOI: 10.1056/NEJMc1408235

TO THE EDITOR: Keramati et al. found that *DYRK1B* mutations were associated with coinheritance of the metabolic syndrome and coronary artery disease. Considering that rare variants as well as common ones in the same gene or locus could be related to the same disease, with a variety of effects,[1,2] we fully endorse the authors' theory that common variants in the *DYRK1B* locus could be associated with the metabolic syndrome in the general population. In the Discussion section of their article, the authors mention that linkage of the *DYRK1B* locus on 19q13 to the metabolic syndrome and type 2 diabetes has been detected in previous genomewide association studies.[3,4] However, the susceptibility loci reported in these studies (the apolipoprotein E [APOE]–C1–C4–C2 gene cluster in the metabolic syndrome and the *PEPD* gene in type 2 diabetes) are considerably distant from the *DYRK1B* locus in a different linkage disequilibrium block. To our knowledge, the *DYRK1B* locus has not thus far been shown to be associated with the metabolic syndrome or coronary artery disease in the general population.

Hiroyuki Morita, M.D., Ph.D.
Issei Komuro, M.D., Ph.D.
University of Tokyo
Tokyo, Japan
hmrt-tky@umin.net

No potential conflict of interest relevant to this letter was reported.

1. Cohen JC, Boerwinkle E, Mosley TH Jr, Hobbs HH. Sequence variations in *PCSK9*, low LDL, and protection against coronary heart disease. N Engl J Med 2006;354:1264-72.
2. Teslovich TM, Musunuru K, Smith AV, et al. Biological, clinical and population relevance of 95 loci for blood lipids. Nature 2010;466:707-13.
3. Kraja AT, Vaidya D, Pankow JS, et al. A bivariate genome-wide approach to metabolic syndrome: STAMPEED consortium. Diabetes 2011;60:1329-39.
4. Cho YS, Chen CH, Hu C, et al. Meta-analysis of genome-wide association studies identifies eight new loci for type 2 diabetes in east Asians. Nat Genet 2012;44:67-72.

DOI: 10.1056/NEJMc1408235

THE AUTHORS REPLY: Mirshahi et al. describe a relatively common nonsynonymous variant in *DYRK1B* (L28P) with an observed allele frequency of 0.53%. In silico analysis indicated that this variant was probably damaging, and it was assumed to be a loss-of-function mutation. A phenomewide association study performed with the use of electronic medical records confirmed their hypothesis and identified this allele as being pro-

tective against several metabolic traits. We agree with their statement that the mutations described in our article represent only one end of the phenotypic spectrum, and we believe there may be many more alleles with loss of function than with gain of function in this gene and most other genes. For example, gain-of-function mutations in proprotein convertase subtilisin/kexin type 9 (PCSK9) have been detected in only a handful of kindreds,[1] whereas loss-of-function protective alleles are much more prevalent in the general population.[2]

We also agree with Mirshahi et al. that the cautious use of electronic medical records is very valuable for the study of population-based genotype–phenotype associations, and we are pleased to see that their analysis independently validated our unbiased findings regarding DYRK1B regulation of metabolism.

As stated by He et al., adipokines are important disease markers for metabolic traits. DYRK1B is expressed at high levels in the brain,[3] and its paralogue Dyrk1A has been shown to play a key role in the central regulation of appetite and body weight by transmitting signals from neuropeptide Y, downstream from ghrelin and leptin.[4] Thus, as with most cases of insulin resistance and obesity, we anticipate consequential alterations in the plasma concentrations of adipokines in *DYRK1B* mutation carriers.[5] We are currently examining food intake and plasma levels of various adipokines in the extended kindreds of *DYRK1B* mutation carriers. The plasma metanephrine, normetanephrine, cortisol, renin, and aldosterone activities were initially measured because of their role in the pathogenesis of multiple metabolic traits ranging from obesity and diabetes mellitus to hypertension; our statement about neurohormones was limited to those measurements.

In our article, we described two novel and extremely rare disease-causing variants of *DYRK1B*, and as stated by Morita and Komuro, we raised the question of whether rare or common variants with a small-to-moderate effect in this gene are linked to the same metabolic traits. However, we predict that future studies will only be able to establish the association of independent rare and subthreshold variants of *DYRK1B* (such as L28P) with metabolic traits. We concur that signals on 19q13 detected in genomewide association studies are most likely linked to the *APOE–C1–C4–C2* gene cluster.

Ali R. Keramati, M.D.
Mohsen Fathzadeh, Ph.D.
Arya Mani, M.D.

Yale University School of Medicine
New Haven, CT
arya.mani@yale.edu

Since publication of their article, the authors report no further potential conflict of interest.

1. Abifadel M, Varret M, Rabès JP, et al. Mutations in PCSK9 cause autosomal dominant hypercholesterolemia. Nat Genet 2003;34:154-6.
2. Cohen JC, Boerwinkle E, Mosley TH Jr, Hobbs HH. Sequence variations in *PCSK9*, low LDL, and protection against coronary heart disease. N Engl J Med 2006;354:1264-72.
3. Tsioras K, Papastefanaki F, Politis PK, Matsas R, Gaitanou M. Functional interactions between BM88/Cend1, Ran-binding protein M and *Dyrk1B* kinase affect cyclin D1 levels and cell cycle progression/exit in mouse neuroblastoma cells. PLoS One 2013; 8(11):e82172.
4. Hong SH, Lee KS, Kwak SJ, et al. Minibrain/Dyrk1a regulates food intake through the Sir2-FOXO-sNPF/NPY pathway in Drosophila and mammals. PLoS Genet 2012;8(8):e1002857.
5. Considine RV, Sinha MK, Heiman ML, et al. Serum immunoreactive-leptin concentrations in normal-weight and obese humans. N Engl J Med 1996;334:292-5.

DOI: 10.1056/NEJMc1408235

CORRECTIONS

Spread of Artemisinin Resistance in *Plasmodium falciparum* Malaria (July 31, 2014;371:411-23). In the Abstract (page 411), in the first sentence of Results, the median parasite clearance half-life in the Democratic Republic of Congo should have been 1.9, rather than 1.8. In the second paragraph of the Discussion (page 419), the third sentence should have read, "With one exception, only one SNP per propeller domain was ever present in 'clonal' infections," rather than "With two exceptions . . . ." The article is correct at NEJM.org.

Thrombus Aspiration during ST-Segment Elevation Myocardial Infarction (October 24, 2013;369:1587-97). In Figure 3 (page 1595), the categories listed under "Age" should have been >65 yr and ≤65 yr, rather than <65 yr and ≥65 yr. The article is correct at NEJM.org.

THE *JOURNAL*'S WEB AND E-MAIL ADDRESSES

To submit a letter to the Editor: authors.NEJM.org

For information about the status of a submitted manuscript: authors.NEJM.org

To submit a meeting notice: meetingnotices@NEJM.org

The *Journal*'s web pages: NEJM.org

Biomaterials 35 (2014) 7839–7850

Contents lists available at ScienceDirect

Biomaterials

journal homepage: www.elsevier.com/locate/biomaterials

Excitation propagation in three-dimensional engineered hearts using decellularized extracellular matrix

Haruyo Yasui [a], Jong-Kook Lee [b, *], Akira Yoshida [a], Teruki Yokoyama [a], Hiroyuki Nakanishi [a], Keiko Miwa [b], Atsuhiko T. Naito [d], Toru Oka [a], Hiroshi Akazawa [d], Junichi Nakai [e], Shigeru Miyagawa [c], Yoshiki Sawa [c], Yasushi Sakata [a], Issei Komuro [d, *]

[a] Department of Cardiovascular Medicine, Osaka University Graduate School of Medicine, Japan
[b] Department of Cardiovascular Regenerative Medicine, Osaka University Graduate School of Medicine, 2-2 Yamada-oka, Suita 565-0871, Japan
[c] Department of Cardiovascular Surgery, Osaka University Graduate School of Medicine, Japan
[d] Department of Cardiovascular Medicine, The University of Tokyo Graduate School of Medicine, 7-3-1 Hongo, Bunkyo-ku, Tokyo 113-8655, Japan
[e] Saitama University Brain Science Institute, Japan

ARTICLE INFO

Article history:
Received 16 May 2014
Accepted 28 May 2014
Available online 20 June 2014

Keywords:
Cardiac tissue engineering
Organ culture
ECM (extracellular matrix)
Scaffold
Electrophysiology

ABSTRACT

Engineering of three-dimensional (3D) cardiac tissues using decellularized extracellular matrix could be a new technique to create an "organ-like" structure of the heart. To engineer artificial hearts functionally comparable to native hearts, however, much remain to be solved including stable excitation-propagation. To elucidate the points, we examined conduction properties of engineered tissues. We repopulated the decellularized hearts with neonatal rat cardiac cells and then, we observed excitation-propagation of spontaneous beatings using high resolution cameras. We also conducted immunofluorescence staining to examine morphological aspects. Live tissue imaging revealed that GFP-labeled-isolated cardiac cells were migrated into interstitial spaces through extravasation from coronary arteries. Engineered hearts repopulated with Ca^{2+}-indicating protein (GCaMP2)-expressing cardiac cells were subjected to optical imaging experiments. Although the engineered hearts generally showed well-organized stable excitation-propagation, the hearts also demonstrated arrhythmogenic propensity such as disorganized propagation. Immunofluorescence study revealed randomly-mixed alignment of cardiomyocytes, endothelial cells and smooth muscle cells. The recellularized hearts also showed disarray of cardiomyocytes and markedly decreased expression of connexin43. In conclusion, we successfully demonstrated that the recellularized hearts showed dynamic excitation-propagation as a "whole organ". Our strategy could provide prerequisite information to construct a 3D-engineered heart, functionally comparable to the native heart.

1. Introduction

Heart diseases are one of the leading causes of mortality worldwide [1]. Despite of recent progress in heart failure treatment, heart transplantation is still considered the final destination therapy for patients with end-stage heart failure refractory to conventional therapies. However, the benefits of heart transplantation are limited due to the shortage of donor hearts. In this context, myocardial regeneration therapy has emerged as a new therapeutic approach to treat severe heart failure. Although several clinical trials have been conducted [2], most therapies involved repairing specific regions of the heart and not the entire heart. Large-scale replacement of cardiac cells is a prerequisite for effective treatment of end-stage heart failure.

For this purpose, a new technique for engineering three-dimensional (3D) organ-like tissue using decellularized extracellular matrix (ECM) was reported for the heart [3], lung [4,5], kidney [6,7], and liver [8]. This technique has already been applied clinically for the engineering of airway [9] or heart valves [10]. A recent paper showed that induced pluripotent stem cell-derived cardiovascular progenitor cells repopulated in a decellularized heart and successfully proliferated, then differentiated into cardiovascular cells [11]. This paper also demonstrated that repopulated induced pluripotent stem cell-derived cells exhibited contraction and electrical activity, but reconstructed heart function was evaluated in the small regions of the heart. To date, only limited information is available regarding the function of a totally engineered organ.

* Corresponding authors.
E-mail address: jlee@cardiology.med.osaka-u.ac.jp (J.-K. Lee).

http://dx.doi.org/10.1016/j.biomaterials.2014.05.080
0142-9612/

Evaluation of arrhythmogenicity as a whole organ will be indispensable to construct a functionally comparable 3D engineered heart. In the present study, we hypothesized that recellularized hearts show well-organized conduction as native hearts. To elucidate the point, we investigated excitation–propagation properties of the recellularized heart by live imaging system using Ca^{2+}-indicating protein (GCaMP2) [31].

2. Materials and methods

2.1. Animals

The study was carried out under the supervision of the Animal Research Committee of Osaka University and in accordance with the Japanese Act on Welfare and Management of Animals. The experimental protocol was approved by the Animal Care and Use Committee of the Osaka University Graduate School of Medicine.

2.2. Perfusion and decellularization of rat hearts

Adult female Wistar rats (10–12-weeks-old) were anesthetized and systemic heparinization was followed by a median sternotomy. After ligating the caval veins, the heart was removed from the chest. A 2-mm cannula was inserted into the ascending aorta to enable Langendorff antegrade coronary perfusion. The right atrium was opened and an incision was made to create an atrial septal defect followed by the ligation of pulmonary artery and veins. Heparinized PBS containing 10 μM ATP was perfused for 15–30 min, followed by perfusion with 0.5% sodium dodecyl sulfate (SDS) in deionized water overnight. After washing with deionized water for 15 min, the heart was perfused with 1% Triton-X100 in deionized water for 30 min, followed by washing with antibiotic-containing PBS (100 U/ml penicillin (Invitrogen, Carlsbad, CA, USA), 100 μg/mL streptomycin (Invitrogen) and 1.25 μg/mL amphotericin B (Sigma–Aldrich, St. Louis, MO, USA)).

2.3. Isolation and preparation of rat neonatal cardiac cells

One-day-old neonatal pups were sacrificed. Their hearts were removed and placed immediately into a Petri dish containing Hank's Balanced Salt Solution (HBSS) on ice. After removing the connective tissue, the hearts were minced with scissors or blades. Trypsin (Neonatal Cardiomyocyte Isolation System, Worthington Biochemical Corporation, Lakewood, NJ, USA) was added to the dish to a final concentration of 50 μg/mL, and incubated overnight at 4 °C. Then, trypsin inhibitor reconstituted with HBSS and collagenase reconstituted with L-15 medium were added to the dish. The tissue was placed in a 37 °C shaker bath for about 35 min. The tissue was then strained through a 100-μm cell strainer and washed with L-15 medium 3 times. After centrifuging the tissue, the pellet was collected and resuspended in 30 mL of M199 (Invitrogen) with 10% FBS (BioWest, Kansas City, MO, USA), 100 U/mL penicillin (Invitrogen), 100 μg/mL streptomycin (Invitrogen), and EGM-2 Single Quots (CC-4176, Lonza, Allendale, NJ, USA) except FBS and GA-1000.

2.4. Recellularization of decellularized hearts

Approximately 1.0 × 10^8 cells were suspended in M199 (Invitrogen) with 10% FBS (BioWest), 100 U/mL penicillin (Invitrogen), 100 μg/mL streptomycin

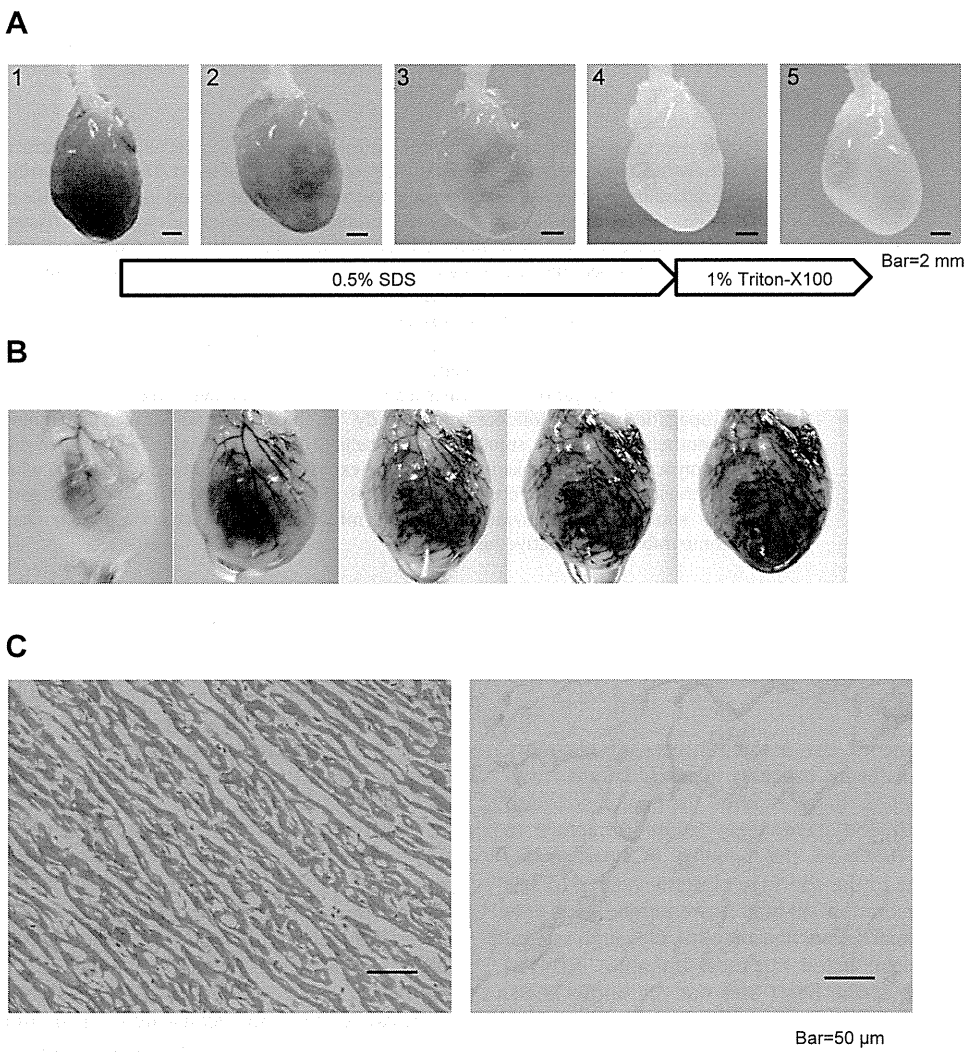

Fig. 1. Decellularization of rat hearts. (A) Macroscopic images of rat hearts during decellularization procedure: before decellularization (1); during 0.5% SDS solution perfusion (2–3); after overnight 0.5% SDS solution perfusion (4); after 1% TritonX-100 solution perfusion (5). Bars indicate 2 mm. (B) Visualization of the architecture of perfused coronary artery of decellularized extracellular matrix. (Evans blue solution was infused through aorta). (C) Microscopic structures of cadaveric (left) and decellularized (right) rat hearts (H–E staining). No nuclear staining was observed in decellularized extracellular matrix. Bars indicate 50 μm.

(Invitrogen), and EGM-2 Single Quots (CC-4176, Lonza) except FBS and GA-1000. Seeded cells consisting of cardiomyocytes, fibroblasts, and endothelial cells were infused through a T-shaped stopcock placed in the line. Recellularized rat hearts were perfused continuously and maintained in 5% CO_2 atmosphere. The culture medium was first changed at day 2 or day 3 with M199 (Invitrogen) containing 10% FBS (BioWest), 100 U/mL penicillin (Invitrogen), 100 μg/mL streptomycin (Invitrogen), and 10 μM cytosine arabinoside (Sigma–Aldrich), but without growth factors and then every 48–72 h.

2.5. Histology and immunofluorescence

We fixed rat cadaveric hearts, decellularized hearts, and recellularized hearts with 4% paraformaldehyde and cryosectioned them. This was followed by hematoxylin–eosin staining and immunostaining. We permeabilized the slides with 0.25% TritonX-100 for 20 min and blocked slides with PBS containing 10% BSA and 0.1% TritonX-100 for 60 min at RT. The samples were incubated overnight at 4 °C with the following primary antibodies: anti-sarcomeric alpha actinin antibody (mouse monoclonal 1:500; Abcam, Cambridge, UK), anti-sarcomeric alpha actinin

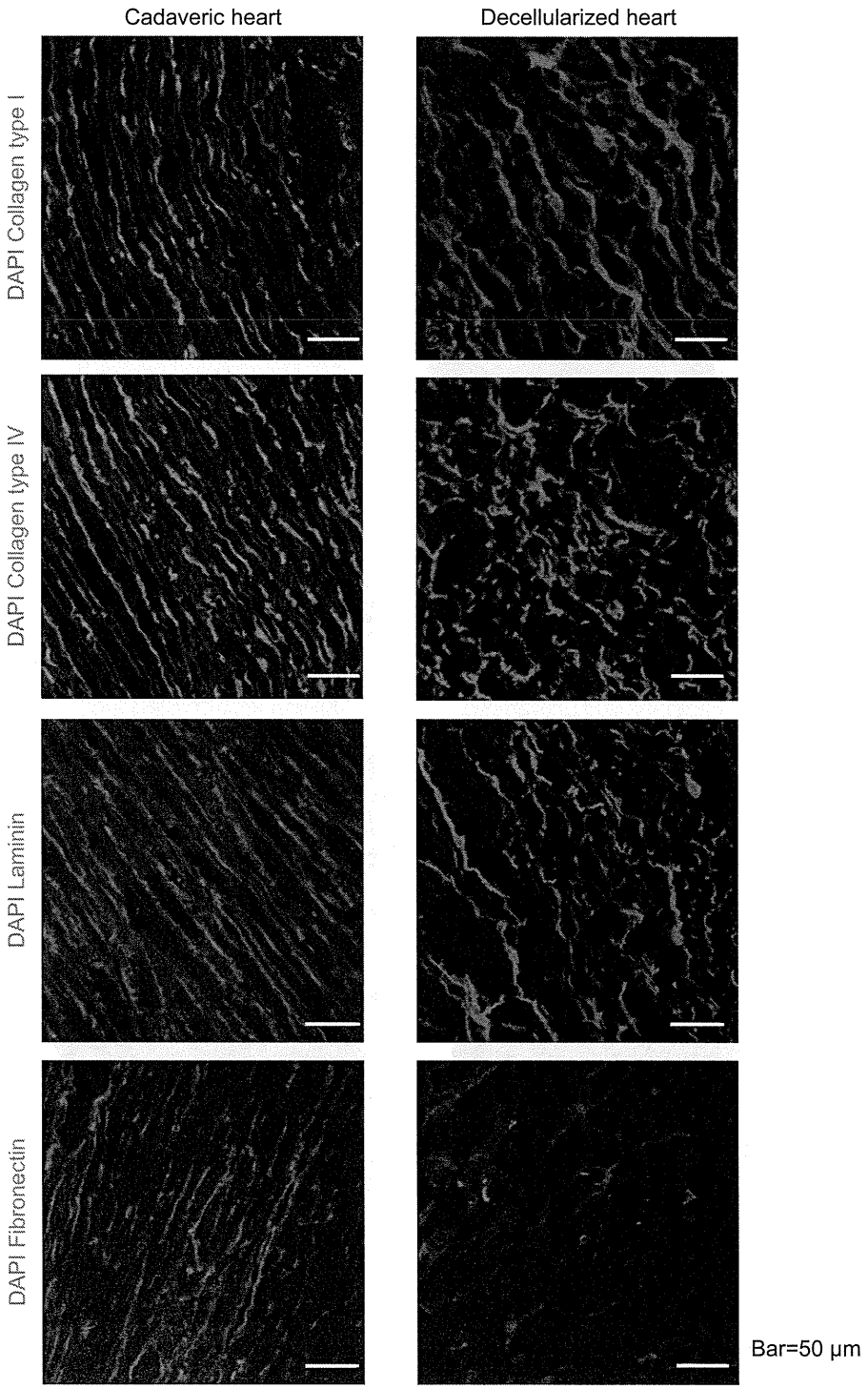

Fig. 2. Immunofluorescent staining of ECM in cadaveric and decellularized rat hearts. Collagen type I, collagen type IV, laminin, and fibronectin were maintained in decellularized (right) rat hearts as in cadaveric (left) hearts, but no nuclei was stained in decellularized (right) rat hearts. Bars indicate 50 μm.

antibody (rabbit polyclonal 1:100; Abcam), anti-laminin antibody (rabbit polyclonal 1:200; Abcam), anti-fibronectin antitibody (rabbit polyclonal 1:200; Abcam), anti-collagen IV antibody (rabbit polyclonal 1:200; Abcam), anti-collagen I antibody (rabbit polyclonal 1:200; Abcam), anti-connexin43 (Cx43) antibody (rabbit polyclonal 1:200; Invitrogen), anti-CD31 antibody (mouse monoclonal 1:100; Abcam), and anti-actin, alpha-smooth muscle-Cy3™ antibody (mouse monoclonal 1:500; Sigma–Aldrich). The samples were then incubated for 1 h with a 1:200 dilution of appropriate secondary antibodies. We embedded the samples in mounting medium containing DAPI (ProLong® Gold Antifade Reagent with DAPI; Invitrogen). Immunofluorescence images were acquired using a microscope (FSX: Olympus, Tokyo, Japan; Biorevo: Keyence, Osaka, Japan).

2.6. Western blot analysis

The frozen samples of an adult rat heart and engineered hearts were homogenized, and proteins were extracted on ice in a buffer solution containing 0.15 M NaCl, 1% NP-40, 50 mM Tris–HCl (pH 8.0), 0.5% sodium deoxycholate, 0.1% SDS and a cocktail of protease inhibitor (Complete, Mini, EDTA-free, Roche, Basel, Switzerland) and phosphatase inhibitor (PhosStop, 20 Tablets, Roche, Basel, Switzerland). Total protein (10 μg/lane) was electrophoresed and separated on an Extra PAGE One Precast Gel (nacalai tesque, Kyoto, Japan). After separation, proteins were transferred onto nitrocellulose membrane sheets (GE Healthcare Japan, Tokyo, Japan). Following transfer, the membrane was blocked in 5% low-fat dry milk in TBS-T at RT for 1 h. Then, the membrane was incubated at 4 °C overnight with following primary antibodies: sarcomeric alpha actinin (mouse monoclonal 1:500; Abcam), myosin heavy chain (MYH) (rabbit polyclonal 1:500; Santa Cruz, Dallas, TX, USA), cardiac troponin I (rabbit polyclonal 1:1000; Abcam), Cx43 (mouse monoclonal 1:1000; Invitrogen), VE-cadherin (goat polyclonal 1:500; Santa Cruz) or GAPDH (rabbit monoclonal 1:5000; Cell Signaling Technology, Danvers, MA, USA). Immunoreactive bands were visualized using an enhanced chemiluminescence (ECL) detection system (Pierce Western Blotting Substrate Plus, Thermo Fisher Scientific, Waltham, MA, USA) and an image analyzer (ImageQuant LAS 4000mini, GE Healthcare Japan).

2.7. Transmission electron microcopy

Decellularized and recellularized hearts were fixed using 2.5% glutaraldehyde (Wako, Osaka, Japan) in 0.1 M phosphate buffer (pH 7.4) through coronary perfusion; they were sectioned into 1-mm pieces and placed in 2.5% glutaraldehyde solution for 2 h. The samples were post-fixed with 1% osmium tetroxide and dehydrated with ethanol. They were embedded in epoxy resin and sectioned into 80 nm slices by

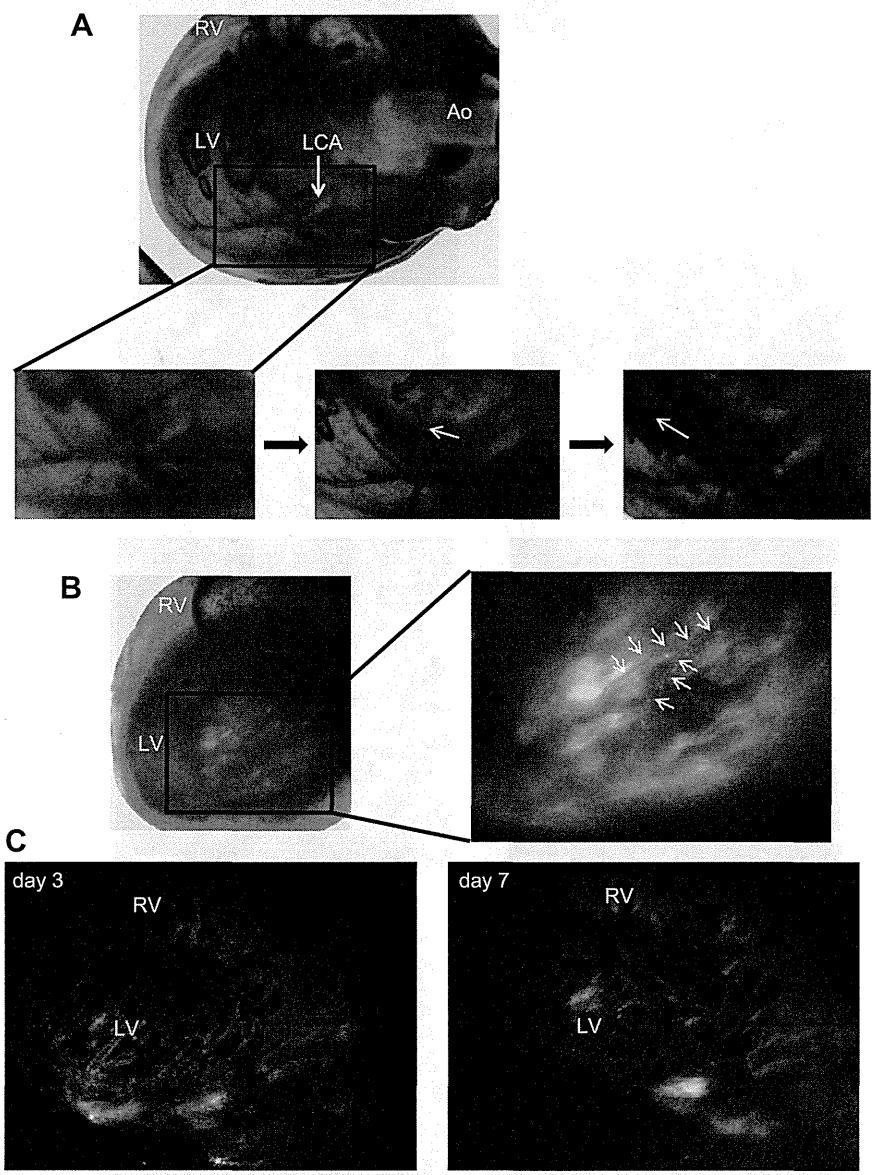

Fig. 3. Extravasation of GFP-labeled neonatal rat cardiac cells. (A) Dispersion of GFP-labeled isolated cardiac cells. GFP-labeled cells were antegradely infused into the coronary artery through aorta (upper panel). Time course of the migration of the cells is shown in magnified images (lower panels): After injection: 4 min (left), 11 min (middle), 16 min (right). The GFP-labeled cells (arrows) migrated into the interstitial spaces through extravasation. (B) At day 2, substantial portion of the seeded cells was observed in the interstitial spaces. Arrows show decellularized vessel structure. The seeded cells existed in the interstitial matrix as well as in the lumens of coronary arteries. (C) GFP-positive cells were retained in the heart for 7 days. Day 3 (left) and day 7 (right). GFP-positive cells were observed throughout the heart but inhomogeneously.

ultramicrotome. Ultra-thin sections were prepared and examined under an electron microscope (H-7650, Hitachi, Tokyo, Japan).

2.8. Transfection of adenovirus encoding GFP and GCaMP2

Isolated neonatal rat cardiac cells were infected with adenovirus encoding GFP and GCaMP2 [31] at a multiplicity of infection (m.o.i.) of 10 and 20, respectively. GFP and GCaMP2 expressing cardiac cells were suspended with the culture medium and injected into the decellularized hearts as described above.

2.9. Electrical and mechanical experiments

Electrocardiograms (ECGs) were recorded in epicardial surface of ventricle. Signals were then digitized through an AD converter (Digidata 1320, Molecular Devices, Sunnyvale, CA, USA) and analyzed with softwares (Axoscope, Molecular Devices; OriginPro, OriginLab Corporation, Northampton, MA, USA). Intraventricular pressures were recorded through a catheter (1.4Fr-Mikro-Tip™ Catheter Transducer, Millar, Bella Vista, NSW, Australia) with an amplifier (PowerLab, AD Instruments Inc., Dunedin, New Zealand).

2.10. Live tissue imaging

We observed recellularized hearts temporarily under a fluorescent stereomicroscope (Leica Microsystems Ltd., Wetzlar, Germany). Recellularized hearts were placed in culture flasks and their fluorescent images were recorded with a GFP-band path filter. Data analysis was performed using custom MALTAB software (MathWorks, Natick, MA, USA). Before fixation, calcium transient (CaT) of the recellularized hearts were optically recorded using a high-resolution CMOS camera (MiCAM02, Brainvision, Tokyo, Japan). Data analysis was performed using custom-made software (BV_Ana, Brainvision). Fast Fourier Transform (FFT) analyses were conducted using software (OriginPro, OriginLab Corporation).

3. Results

3.1. Decellularization of adult rat hearts

Perfusion of 0.5% SDS and subsequent application of 1% Triton-X100 removed all the cellular components from the hearts, leaving behind the extracellular matrices (Fig. 1A). Histological

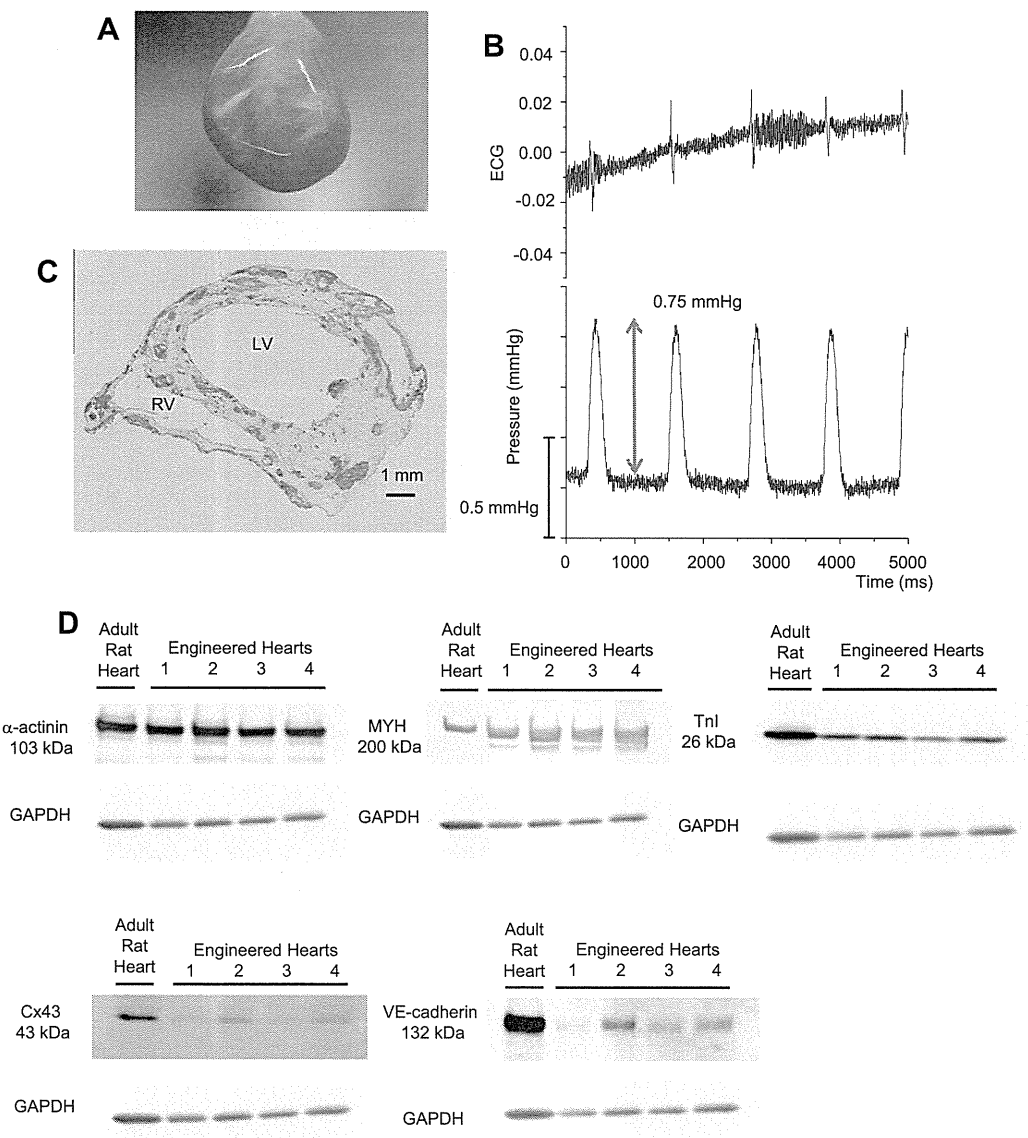

Fig. 4. Properties of recellularized hearts. (A) An image of a recellularized rat heart showing spontaneous beating. (Supplemental movie is available as Movie S2). (B) Real-time tracings of ECG and ventricular pressure are shown. The tracings of ECG and manometry were synchronized and intraventricular pressure was approximately 0.75 mmHg. (C) A microscopic image of a recellularized rat heart in transverse section (H–E staining). Inhomogeneous distribution of seeded cells was observed throughout the heart. Bar indicates 1 mm. (D) Western blot analysis of heart extracts. An adult rat heart and 4 engineered hearts were subjected to western blot analysis. Note the faint expression of VE-cadherin and connexin43 (Cx43) in engineered hearts compared to adult rat heart, in contrast to the abundant expression of sarcomeric alpha actinin, myosin heavy chain (MYH) and cardiac troponin I (TnI), both in engineered and native adult rat hearts.

evaluation revealed an absence of nuclei in the decellularized hearts (Figs. 1C and 2). Immunofluorescent staining demonstrated that collagen I, collagen IV, laminin, and fibronetin remained within the decellularized heart matrix (Fig. 2). Antegrade coronary perfusion with Evans blue dye delineated the extracellular structures of the main coronary arteries (Fig. 1B). The arterial remnants were abruptly terminated. Detailed observation revealed that decellularization procedure destroyed the entire vessel walls in the peripheral arterioles but not in the proximal arteries. This finding may be attributed to sparse extracellular matrices in the peripheral arterioles.

3.2. Whole-heart engraftment of GFP-labeled cells

Live tissue fluorescence imaging of the GFP-labeled seeded cells after antegrade infusion through coronary arteries revealed that the GFP-labeled cardiac cells had extended through the lumens of decellularized coronary arteries into the interstitial spaces at the tip of the remnant coronary arteries (Fig. 3A and Supplementary Movie 1). At day 3, inhomogeneous distribution of the GFP-positive cells was observed throughout the heart tissues. The seeded cells were found in the lumens of coronary arteries as well as in the interstitial matrix (Fig. 3B, C). We also observed that the GFP-positive cells were retained in the heart during the entire observation period (Fig. 3C).

Supplementary video related to this article can be found at http://dx.doi.org/10.1016/j.biomaterials.2014.05.080.

3.3. Recellularization of the decellularized hearts with cardiac cells of neonatal rats

We seeded decellularized rat hearts with freshly isolated neonatal cardiac cells through antegrade coronary perfusion. As the cell isolation procedure did not include techniques such as "pre-plating" method to remove specific cardiac cell types, both cardiomyocytes and other types of cells such as fibroblasts were seeded into the decellularized heart. The 3D organ-like culture was maintained for 8–30 days. Recellularized hearts started spontaneous contraction 2–3 days after recellularization, which continued for 8–30 days (Fig. 4A and Supplementary Movie 2). We

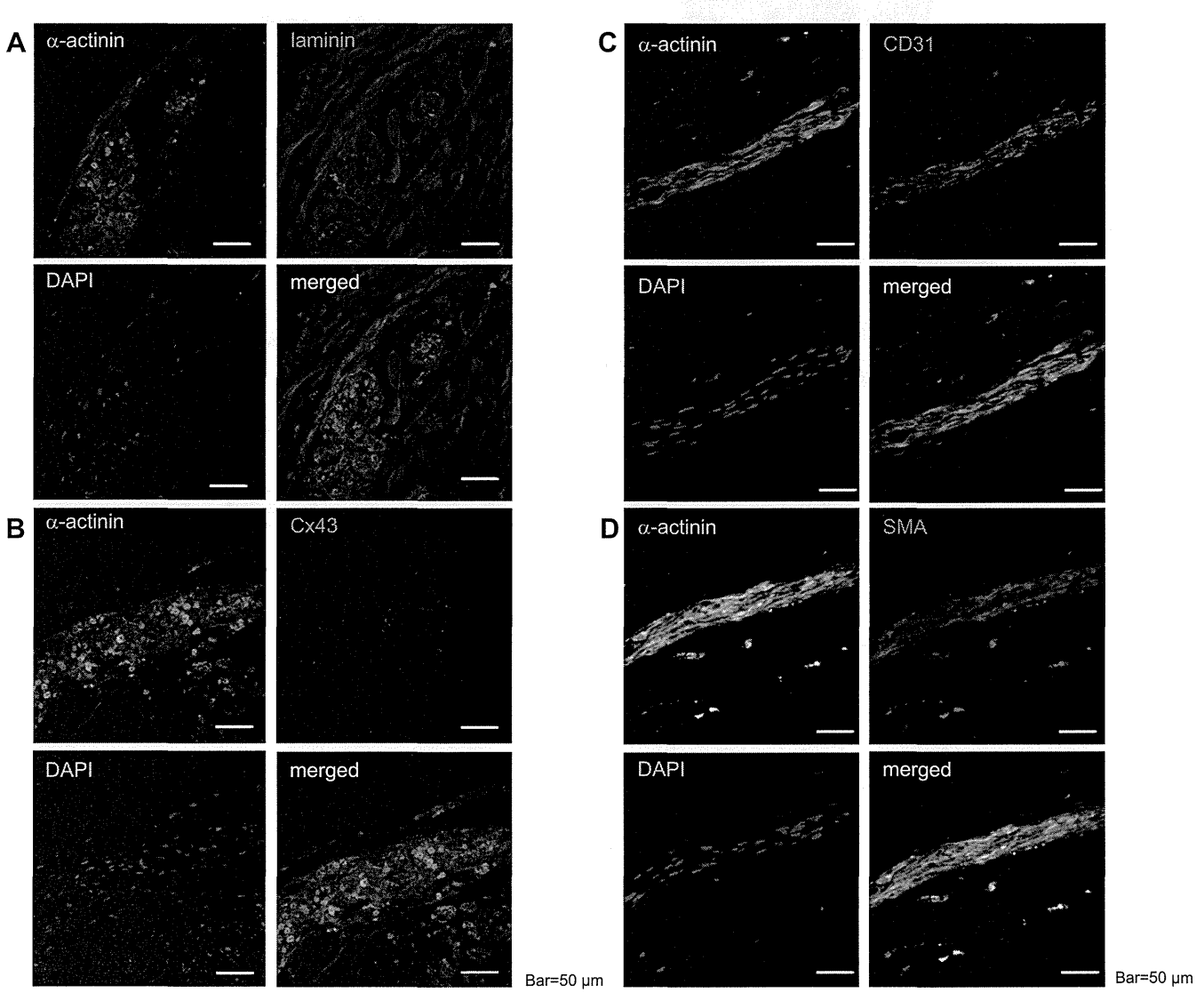

Fig. 5. Immunofluorescence study of recellularized hearts. (A) Sarcomeric alpha actinin-positive cells were surrounded by laminin-positive ECM. (B) Cx43 was sparsely observed among sarcomeric alpha actinin-positive cells. (C), (D) Random alignment of cardiomyocytes, endothelial cells, and smooth muscle cells. The mixture of different cells was observed. Alpha-actinin, CD31, and smooth-muscle-actin were used as cardiac, endothelial, and smooth muscle cell markers, respectively.

recorded electrocardiogram (ECG) and intraventricular pressure. The synchronized tracings of ECG and pressure were shown in Fig. 4B. Microscopic observation revealed that seeded cells adhered inhomogeneously to the decellularized ECM (Fig. 4C). We further examined whether cardiac proteins existed in recellularized hearts by western blot analysis (Fig 4D). As a result, cardiac contractile proteins, including sarcomeric alpha actinin, MYH and cardiac troponin I (TnI), were abundantly observed, while VE-cadherin and Cx43 were only faintly detected in engineered hearts compared to an adult rat heart. Among the seeded cells, sarcomeric alpha actinin positive cells were detected in the ventricles; these cells were surrounded by laminin-positive ECM (Fig. 5A). Although regions of the alpha actinin-positive cells were accompanied by Cx43, the expression was faint, which indicated that intercellular conduction might be immature as compared to adult hearts (Fig. 5B). An immunofluorescence study revealed a randomly-mixed alignment of cardiomyocytes, endothelial cells, and smooth muscle cells stained with alpha actinin, CD31, and smooth muscle (sm)-actin, respectively (Fig. 5C, D). CD31-positive cells and sm-actin-positive cells were not necessarily localized to decellularized vessel-like structures. Transmission Electron Microscope observations showed that the decellularized hearts preserved collagen fibers well in the ECM (Fig. 6A) and the recellularized hearts demonstrated the presence of sarcomeric structures surrounded by ECM (Fig. 6B).

Supplementary video related to this article can be found at http://dx.doi.org/10.1016/j.biomaterials.2014.05.080.

3.4. Excitation-propagation of recellularized hearts

Engineered hearts seeded with GCaMP2-expressing cardiac cells showed spontaneous beating within 2–3 days after recellularization, at which point they were subjected to optical imaging experiments. We observed that spontaneous excitations were generally well aligned and stably propagated in the engineered heart tissues (Fig. 7A and Supplementary Movie 3). Fig. 7A shows the representative images of propagation sequences in an engineered heart. Excitation seemed to emerge in the lateral wall of left ventricle (LV) and propagated through the free LV wall. Isochrone map of the propagating CaT suggested inhomogeneous conduction in substantial areas (Fig. 7C). Conduction velocity (CV) was an order of magnitude or slower (approximately 0.5–5 cm/s) compared to normal adult rat hearts.

Supplementary video related to this article can be found at http://dx.doi.org/10.1016/j.biomaterials.2014.05.080.

3.5. Arrhythmogenicity of recellularized heart tissues

To examine the underlying mechanisms of arrhythmogenesis in the engineered heart tissues and the time-course of maturation in electrical properties, live tissue fluorescence video imaging was employed. We used FFT analysis to examine the synchronicity. Spontaneous excitation of CaT recorded at the three discrete points in the engineered heart tissues were subjected to FFT analysis. In the sample of the first group, during spontaneous beating, the

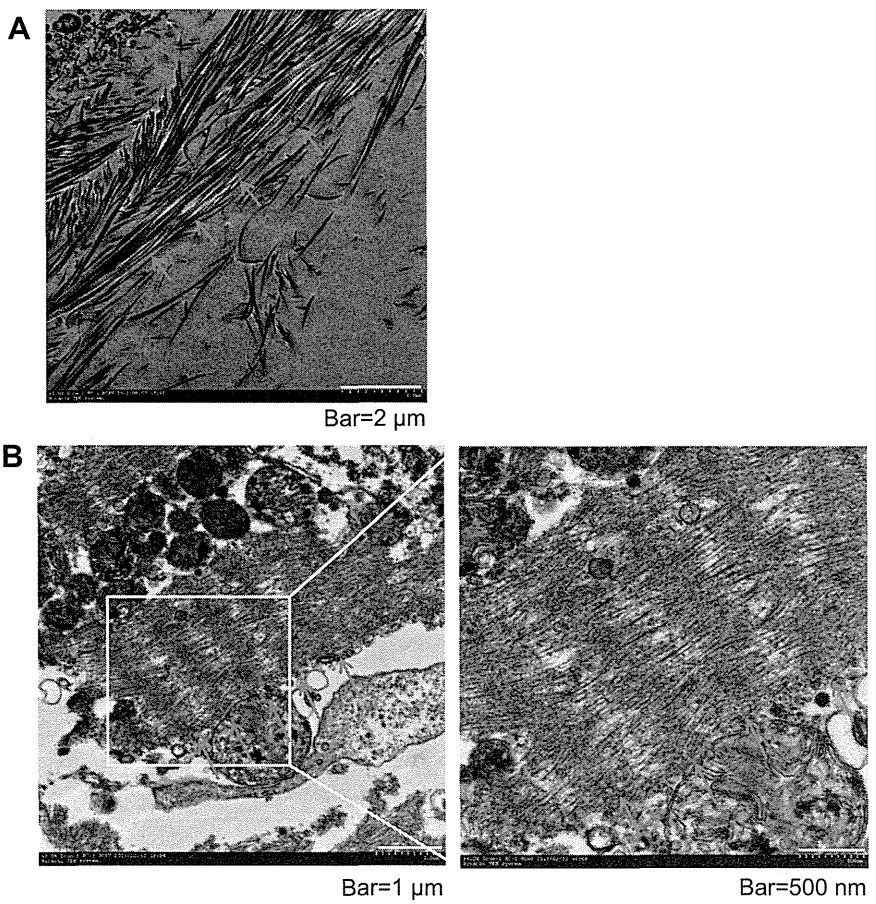

Fig. 6. Ultrastructure of decellularized and recellularized rat hearts by transmission electron microscopy. (A) Ultrastructure of a decellularized heart. Collagen fibers (arrows) in the ECM were well preserved after decellularization procedure. (B) Ultrastructure of a recellularized heart. Arrows show cells with well-organized stria. Cardiac cells seemed to be surrounded by ECM.

entire heart tissues were well-synchronized (Fig. 8A–E and Supplementary Movie 4). Isochrone map showed that excitation propagated rapidly through the left ventricle (Fig. 8D). Frequency analysis showed similar frequency profile pattern at each point (Fig. 8E). On the other hand, in the sample of the second group, although substantial parts of the tissues showed well-organized propagation of excitation, unsynchronized beatings were also observed around ROI-2 (Fig. 9A–E and Supplementary Movie 5). Isochrone map of the propagating CaT showed that initial activation generated from two distinct sites at basal and apical parts of the heart (Fig. 9D). The frequency profiles were accordingly similar at ROI-1 and ROI-3, but not at ROI-2 (Fig. 9E). These observations suggested that there were multiple re-entry like circuits. The sample of the third group exhibited markedly arrhythmogenic characteristics. The heart tissues showed spontaneous contraction, but each region did not show synchronization (Fig. 10A–E and Supplementary Movie 6). Conduction between left and right sides of the heart was hardly observed (Fig. 10D).

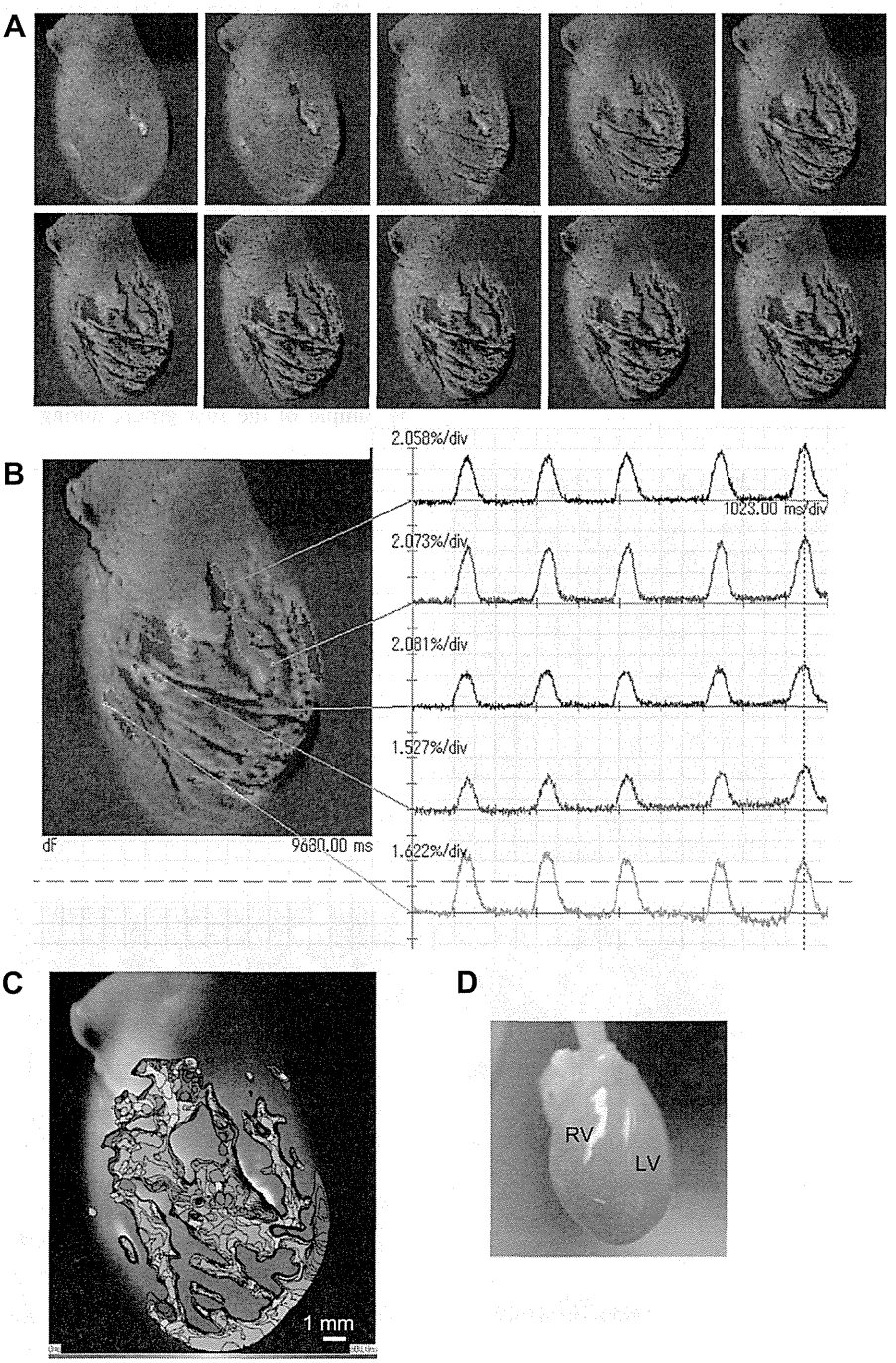

Fig. 7. Propagation of the intracellular calcium transient (CaT) in a recellularized heart. (A) Sequential images in spontaneous beating (every 40 ms). Optical images showed excitation-propagation throughout epicardial surface of the recellularized heart. (B) Detection of the intracellular CaT. (C) Isochrone map (in 10 ms color-coded intervals) of the propagating CaT. Isochrone map suggested inhomogeneous propagation in substantial areas. (D) Anatomical features of the recellularized heart from a frame of video file.

Frequency analysis showed that ROI-1, -2, and -3 beat independently (Fig. 10E). These observations suggested each region had automaticity although cardiac cells were continuously present among ROI-1, -2, and -3.

Supplementary video related to this article can be found at http://dx.doi.org/10.1016/j.biomaterials.2014.05.080.

4. Discussion

In the present study, we successfully constructed 3D engineered hearts by recellularizing adult rat decellularized hearts with neonatal rat cardiac cells, and demonstrated the excitation and propagation properties of 3D engineered heart tissues as an "organ".

For myocardial regeneration therapy of severe heart failure, sufficient wall thickness is required for engrafted cardiac tissues to assist pumping function of the failing hearts. To elucidate the point, several attempts have been made such as "3D cardiac patch" with promoted maturation from ES cell-derived cardiomyocytes [12] or "multi-layered cardiac cell sheets" based on temperature-responsive cell culture dishes [13]. Despite of these efforts, there still remains a limitation in oxygen delivery to thick myocardial tissues, and thus the thickness of the engineered cardiac tissues is confined to approximately 200 μm or less [14,15]. Recent techniques to engineer cardiac tissues with perfusable blood vessels have made thicker vascularized cardiac tissues feasible, which showed spontaneous beating and were transplanted with blood vessel anastomoses [16]. Eschenhagen and Zimmermann

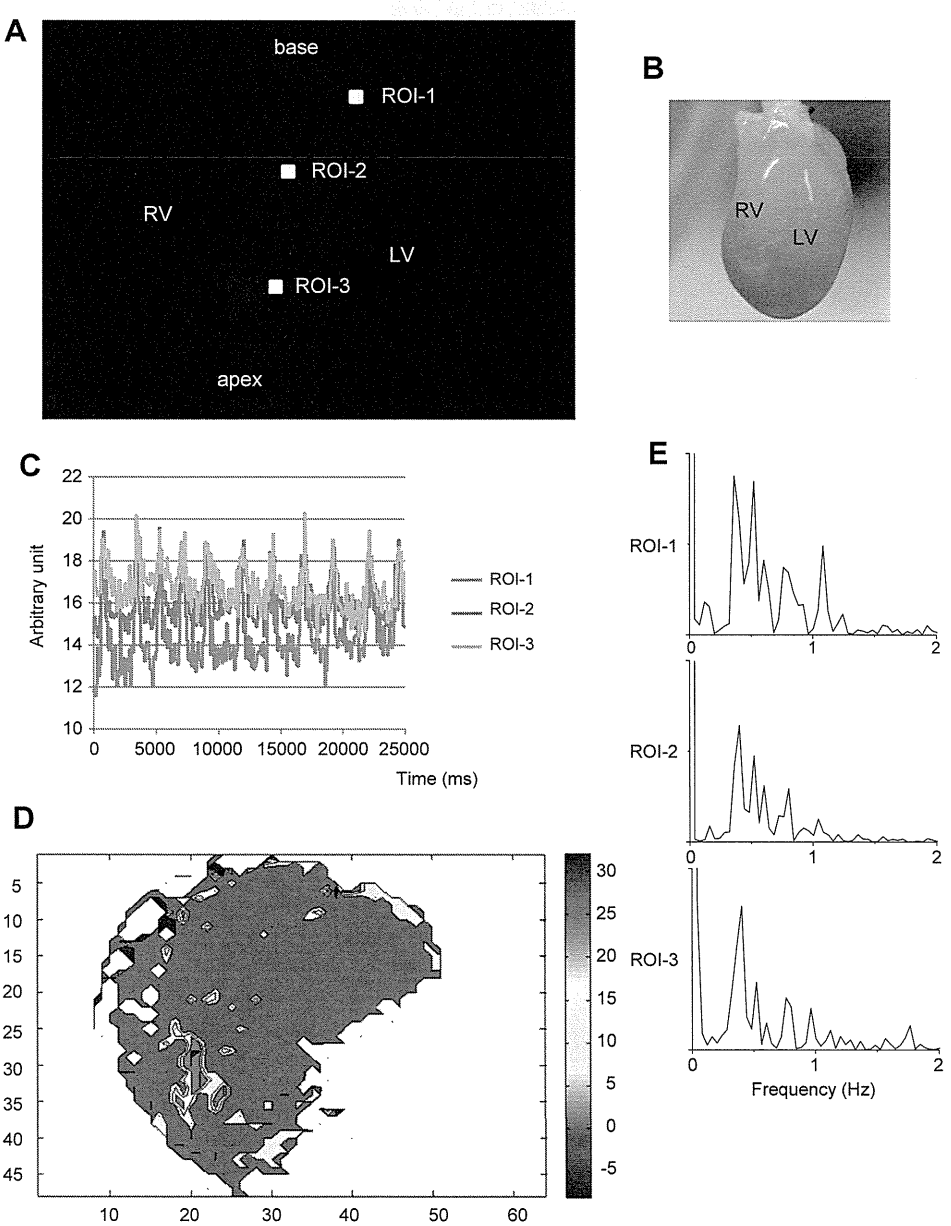

Fig. 8. Propagation of recellularized heart tissues ('well-synchronized' group). (A) Detection of the intracellular CaT driven by local propagation of electrical activity (ROI-1, -2, and -3) in the sample 1. (B) Anatomical features of the recellularized heart from a frame of video file. (C) Intracellular CaT at each site. We observed well-organized conduction of stable excitation in substantial areas of the engineered heart tissues. (D) Isochrone map of the propagating CaT. Note that excitation rapidly propagated throughout the left ventricle. (E) Fast Fourier Transform (FFT) analysis. Note that each site showed similar frequency pattern.

engineered cardiac tissues using a mixture of collagen I, ECM proteins (Matrigel®) and neonatal rat cardiomyocytes into molds; their constructs were intensively interconnected [17]. Their 1–4-mm-thick engineered heart tissue grafts improved the systolic and diastolic functions on implantation in infarcted rat hearts [18].

However, they could not preserve the large-scaled 3D architectures and natural matrix components of the heart. In this context, decellularized whole hearts may act as niches for repopulated cells and vessels for supplying the nutrients to the engineered myocardial constructs. It was indicated that ECM components and preserved mechanical properties of the decellularized heart had directed differentiation of the stem/progenitor cells into the cardiac lineage [19]. This observation also suggests that decellularized heart matrix may therefore be a promising alternative to synthetic scaffolds and a foundation for regenerative efforts for 3D tissue engineering [20].

Previous attempts have revealed that engineered myocardial tissues are not fully synchronized in the small regions of the whole hearts [11,21]. We achieved partial synchronization of significant regions of the heart, but also observed regions which beat independently. Synchronicity is an important factor for the construction of a transplantable artificial organ, since asynchronous regions impair the contractility, as well as potentially increase the risk of lethal cardiac arrhythmias. The calculated CV in our engineered heart tissues was markedly decreased (approximately 5 cm/s) as compared to that reported previously in an adult rat heart [22,23]

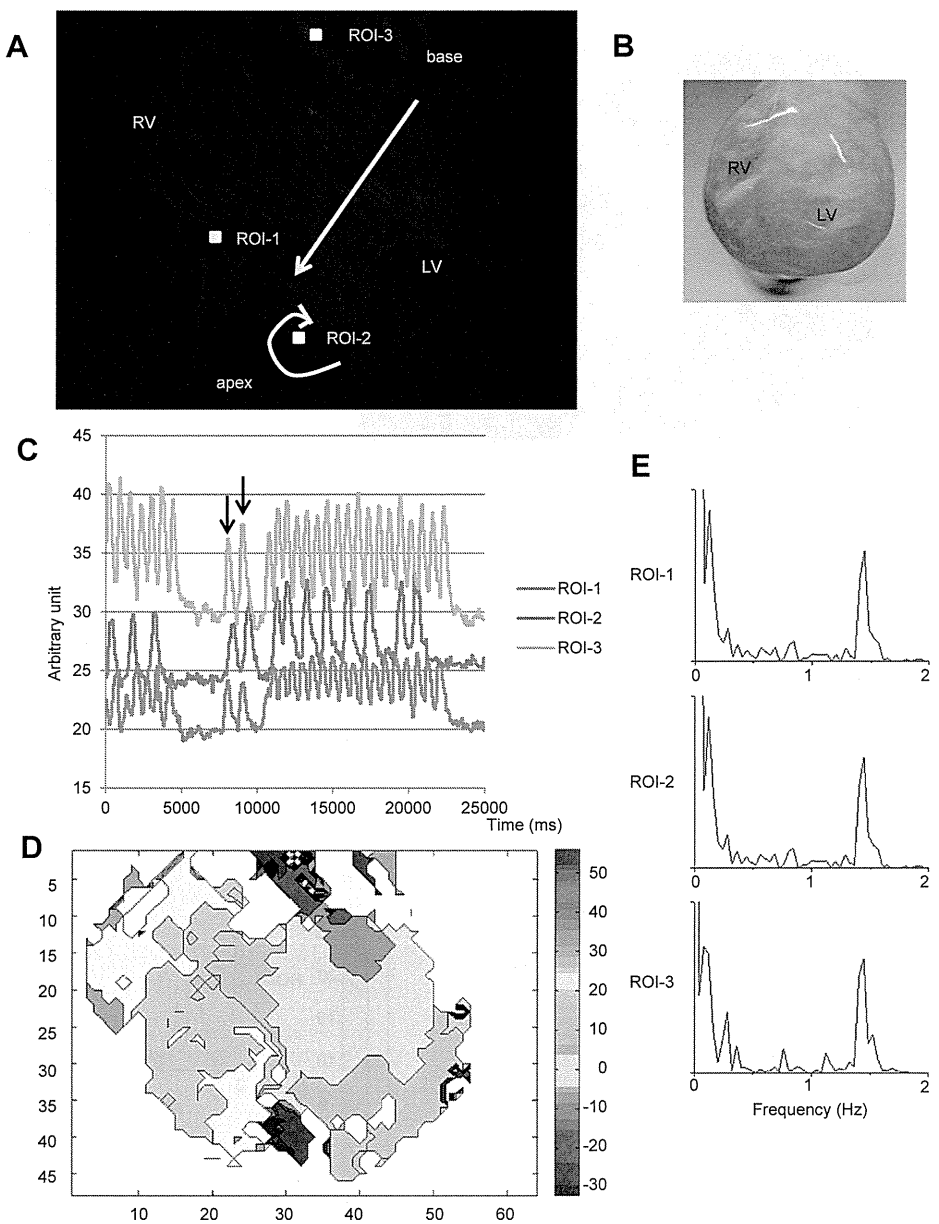

Fig. 9. Propagation of recellularized heart tissues ('unsynchronized' group). (A) Detection of the intracellular CaT driven by local propagation of electrical activity (ROI-1, -2, and -3) in the sample 2. (B) Anatomical features of the recellularized heart from a frame of video file. (C) Intracellular CaT at each site. Propagation of most parts showed the unsynchronized pattern. After 2 beats (arrows), there was a pause, and another wave emerged from the bottom of the heart and collided with the preceding wave. (D) Isochrone map of the propagating CaT. Note that initial activation generated from two distinct sites at basal and apical parts of the heart. (E) FFT analysis. The frequency profiles were similar at ROI-1 and ROI-3, but not at ROI-2. This suggested that at least two excitation-propagation existed.

or in an *in vitro* cultured neonatal rat cardiomyocyte (NRCM), whereas it was similar to that of NRCM with Cx43 mutation [24]. Slow conduction and electrical instability were more apparent in the whole heart. The mixture of automaticity from multiple sites and multiple re-entry leads to arrhythmogenic propensity and obstructs adequate contraction. To create a whole heart with sufficient contraction, electrophysiological evaluation of the whole heart is essential.

Our engineered heart showed a marked decrease in expression of Cx43, which is one of the reasons why our engineered constructs showed slow conduction and electrical instability as well as sparse adhesion of the repopulated cardiomyocytes. This might be improved by overexpressing Cx43 in the engineered cells. Immunofluorescence study revealed randomly mixed alignment of cardiomyocytes, endothelial cells, and smooth muscle cells stained with alpha-actinin, CD31, and sm-actin, respectively; these cells were located close to one another. The mixture of different cells may inhibit smooth electrical conduction. Although these cells were present simultaneously, it is possible that previously resident cadiomyocytes attracted other endothelial cells and attempted to

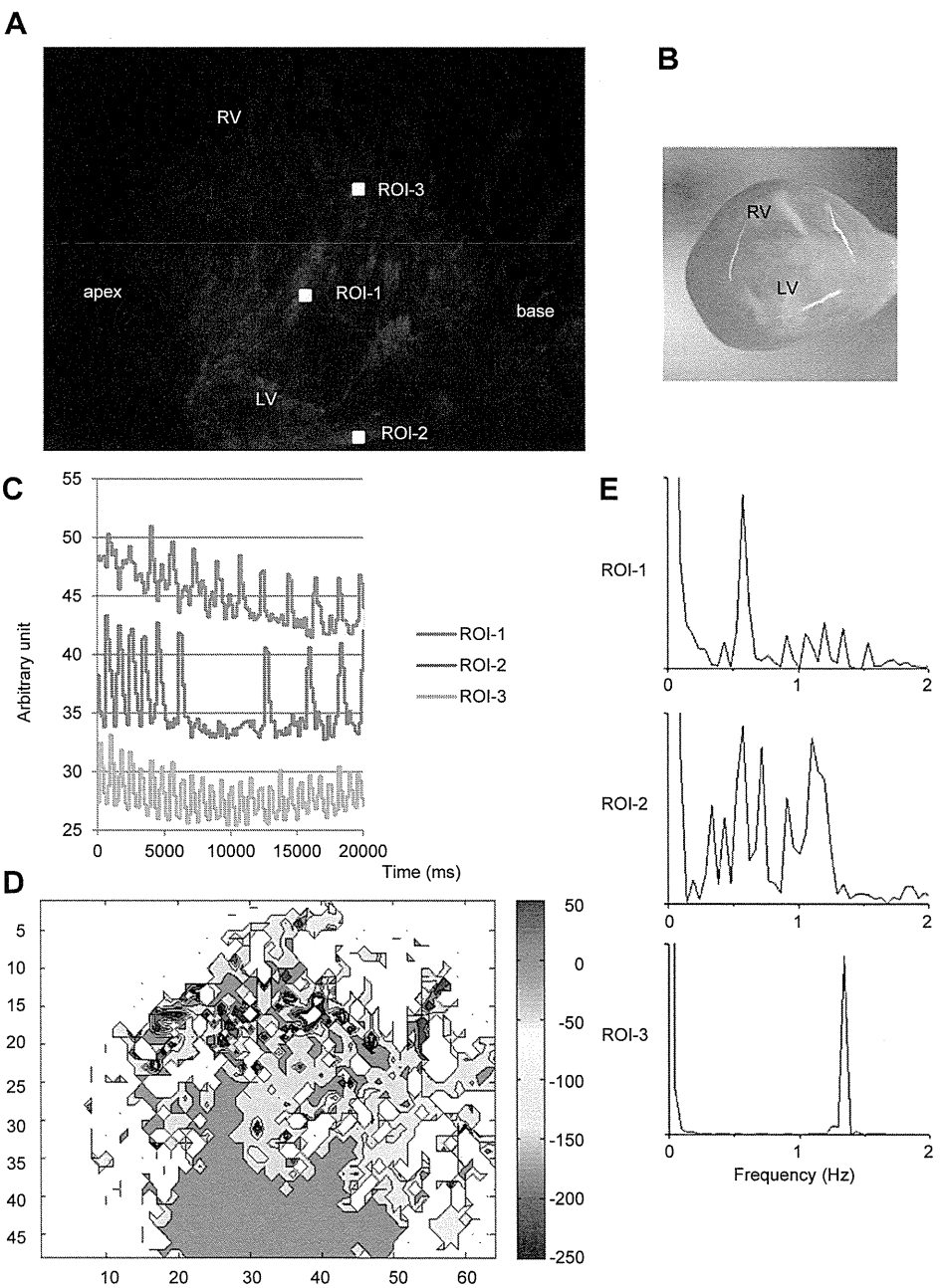

Fig. 10. Propagation of recellularized heart tissues ('disorganized' group). (A) Detection of the intracellular CaT driven by local propagation of electrical activity (ROI-1, -2, and -3) in the sample 3. (B) Anatomical features of the recellularized heart from a frame of video file. The heart sample is shown in the same direction with panels A and D. (C) Intracellular CaT at each site. We recorded disorganized propagation of asynchronous excitation with multiple origins, indicating automaticity. (D) Isochrone map of the propagating CaT. Note that left and right sides of the heart showed distinct automaticity and that conduction between these distinct sites was hardly observed. (E) FFT analysis. Note that each site showed different frequency pattern.

form capillary blood vessels. Cross-talk between endothelial cells and cardiomyocytes regulates not only early cardiac development but also adult cardiomyocyte contraction [25]. Also, it has been reported that the inductive signaling from endothelial cells plays an important role in cardiac conduction system development [26]. The co-existence of endothelial cells and cardiomyocytes may be compatible with this endothelial–cardiomyocyte interaction in the native heart. The density of laminin was high around the resident cardiomyocytes. The finding suggests that cardiomyocytes may produce laminin autonomously in addition to the natural matrix and adapt themselves at the resided space in the matrix. Supplementation with additional extracellular matrices could be possible experiments to attempt.

Extraction of the cadaveric heart *per se* could be potential controversies due to the notion on the death. For example, fabrication of scaffolds analogous to biological tissues using advanced technology such as 3D bioprinting technique may provide clues to solve the issue [27]. The technique has already been applied in various biological tissues including heart valves [28,29] and cartilage [30]. In this regard, 3D bioprinting could be a possible arsenal for heart regeneration in the future, however, arrhythmogenic evaluation as a whole organ will be still essential to create a sufficiently functional heart.

5. Conclusion

We engineered 3D hearts by recellularizing adult rat decellularized hearts with neonatal rat cardiac cells and observed excitation-propagation of spontaneous beatings of the recellularized heart tissues as an "organ". We observed disorganized asynchronous excitation arising from multiple origins while the engineered 3D heart tissues generally showed well-organized stable conduction. Although previous studies have shown the electrophysiological characteristics of 3D engineered heart tissues, those were only limited to the small area of the heart. In the present study, we clearly presented excitation and propagation properties of the entire heart tissues as an "organ". To construct functionally comparable and transplantable artificial heart, our strategy may be beneficial in the evaluation of the arrhythmogenic propensity, and it is necessary to establish the technique to engineer 3D heart tissues with stable excitation-propagation propensity as an organ.

Acknowledgments

We thank Nobu Miyakawa (Osaka University) for technical support of neonatal rat cardiac cell isolation and rat heart decellularization and Ken Shimono, Ph.D. (Panasonic Corporation) for data analysis using MALTAB software.

This work was supported in part by the Japan Society for the Promotion of Science [(Grant-in-Aid for Scientific Research (B), 26293188) (J.L.)].

References

[1] Lozano R, Naghavi M, Foreman K, Lim S, Shibuya K, Aboyans V, et al. Global and regional mortality from 235 causes of death for 20 age groups in 1990 and 2010: a systematic analysis for the Global Burden of Disease Study 2010. Lancet 2012;380:2095–128.
[2] Pfister O, Della Verde G, Liao R, Kuster GM. Regenerative therapy for cardiovascular disease. Transl Res 2014;163:307–20.
[3] Ott HC, Matthiesen TS, Goh S-K, Black LD, Kren SM, Netoff TI, et al. Perfusion-decellularized matrix: using nature's platform to engineer a bioartificial heart. Nat Med 2008;14:213–21.
[4] Ott HC, Clippinger B, Conrad C, Schuetz C, Pomerantseva I, Ikonomou L, et al. Regeneration and orthotopic transplantation of a bioartificial lung. Nat Med 2010;16:927–33.
[5] Petersen TH, Calle EA, Zhao L, Lee EJ, Gui L, Raredon MB, et al. Tissue-engineered lungs for in vivo implantation. Science 2010;329:538–41.
[6] Song JJ, Guyette JP, Gilpin SE, Gonzalez G, Vacanti JP, Ott HC. Regeneration and experimental orthotopic transplantation of a bioengineered kidney. Nat Med 2013;19:646–51.
[7] Nakayama KH, Batchelder CA, Lee CI, Tarantal AF. Decellularized rhesus monkey kidney as a three-dimensional scaffold for renal tissue engineering. Tissue Eng Part A 2010;16:2207–16.
[8] Uygun BE, Soto-Gutierrez A, Yagi H, Izamis M-L, Guzzardi M a, Shulman C, et al. Organ reengineering through development of a transplantable recellularized liver graft using decellularized liver matrix. Nat Med 2010;16:814–20.
[9] Macchiarini P, Jungebluth P, Go T, Asnaghi MA, Rees LE, Cogan TA, et al. Clinical transplantation of a tissue-engineered airway. Lancet 2008;372:2023–30.
[10] Cebotari S, Tudorache I, Ciubotaru A, Boethig D, Sarikouch S, Goerler A, et al. Use of fresh decellularized allografts for pulmonary valve replacement may reduce the reoperation rate in children and young adults: early report. Circulation 2011;124:S115–23.
[11] Lu T-Y, Lin B, Kim J, Sullivan M, Tobita K, Salama G, et al. Repopulation of decellularized mouse heart with human induced pluripotent stem cell-derived cardiovascular progenitor cells. Nat Commun 2013;4:2307.
[12] Zhang D, Shadrin IY, Lam J, Xian H-Q, Snodgrass HR, Bursac N. Tissue-engineered cardiac patch for advanced functional maturation of human ESC-derived cardiomyocytes. Biomaterials 2013;34:5813–20.
[13] Shimizu T, Yamato M, Isoi Y, Akutsu T, Setomaru T, Abe K, et al. Fabrication of pulsatile cardiac tissue grafts using a novel 3-dimensional cell sheet manipulation technique and temperature-responsive cell culture surfaces. Circ Res 2002;90:e40.
[14] Radisic M, Malda J, Epping E, Geng W, Langer R, Vunjak-Novakovic G. Oxygen gradients correlate with cell density and cell viability in engineered cardiac tissue. Biotechnol Bioeng 2006;93:332–43.
[15] Radisic M, Euloth M, Yang L, Langer R, Freed LE, Vunjak-Novakovic G. High-density seeding of myocyte cells for cardiac tissue engineering. Biotechnol Bioeng 2003;82:403–14.
[16] Sekine H, Shimizu T, Sakaguchi K, Dobashi I, Wada M, Yamato M, et al. In vitro fabrication of functional three-dimensional tissues with perfusable blood vessels. Nat Commun 2013;4:1399.
[17] Zimmermann W-H, Schneiderbanger K, Schubert P, Didie M, Munzel F, Heubach JF, et al. Tissue engineering of a differentiated cardiac muscle construct. Circ Res 2002;90:223–30.
[18] Zimmermann W-H, Melnychenko I, Wasmeier G, Didié M, Naito H, Nixdorff U, et al. Engineered heart tissue grafts improve systolic and diastolic function in infarcted rat hearts. Nat Med 2006;12:452–8.
[19] Ng SLJ, Narayanan K, Gao S, Wan ACA. Lineage restricted progenitors for the repopulation of decellularized heart. Biomaterials 2011;32:7571–80.
[20] Song JJ, Ott HC. Organ engineering based on decellularized matrix scaffolds. Trends Mol Med 2011;17:424–32.
[21] Kadota S, Minami I, Morone N, Heuser JE, Agladze K, Nakatsuji N. Development of a reentrant arrhythmia model in human pluripotent stem cell-derived cardiac cell sheets. Eur Heart J 2013;34:1147–56.
[22] Parikh A, Patel D, McTiernan CF, Xiang W, Haney J, Yang L, et al. Relaxin suppresses atrial fibrillation by reversing fibrosis and myocyte hypertrophy and increasing conduction velocity and sodium current in spontaneously hypertensive rat hearts. Circ Res 2013;113:313–21.
[23] Hardziyenka M, Campian ME, Verkerk AO, Surie S, van Ginneken ACG, Hakim S, et al. Electrophysiologic remodeling of the left ventricle in pressure overload-induced right ventricular failure. J Am Coll Cardiol 2012;59:2193–202.
[24] Kizana E, Chang CY, Cingolani E, Ramirez-Correa G a, Sekar RB, Abraham MR, et al. Gene transfer of connexin43 mutants attenuates coupling in cardiomyocytes: novel basis for modulation of cardiac conduction by gene therapy. Circ Res 2007;100:1597–604.
[25] Hsieh PCH, Davis ME, Lisowski LK, Lee RT. Endothelial-cardiomyocyte interactions in cardiac development and repair. Annu Rev Physiol 2006;68:51–66.
[26] Tian Y, Morrisey EE. Importance of myocyte-nonmyocyte interactions in cardiac development and disease. Circ Res 2012;110:1023–34.
[27] Derby B. Printing and prototyping of tissues and scaffolds. Science 2012;338:921–6.
[28] Duan B, Kapetanovic E, Hockaday L a, Butcher JT. Three-dimensional printed trileaflet valve conduits using biological hydrogels and human valve interstitial cells. Acta Biomater 2014;10:1836–46.
[29] Hockaday L a, Kang KH, Colangelo NW, Cheung PYC, Duan B, Malone E, et al. Rapid 3D printing of anatomically accurate and mechanically heterogeneous aortic valve hydrogel scaffolds. Biofabrication 2012;4:035005.
[30] Cui X, Breitenkamp K, Finn MG, Lotz M, D'Lima DD. Direct human cartilage repair using three-dimensional bioprinting technology. Tissue Eng Part A 2012;18:1304–12.
[31] Tallini YN, Ohkura M, Choi BR, Ji G, Imoto K, Doran R, et al. Imaging cellular signals in the heart in vivo: cardiac expression of the high-signal Ca^{2+} indicator GCaMP2. Proc Natl Acad Sci U S A 2006;103(12):4753–8.

ORIGINAL RESEARCH

American Heart Association | American Stroke Association.

Mitochondrial Aldehyde Dehydrogenase 2 Plays Protective Roles in Heart Failure After Myocardial Infarction via Suppression of the Cytosolic JNK/p53 Pathway in Mice

Aijun Sun, PhD;* Yunzeng Zou, MD, PhD;* Ping Wang, PhD;* Danling Xu, PhD;* Hui Gong, PhD;* Shijun Wang, PhD; Yingjie Qin, PhD; Peng Zhang, MD; Yunqin Chen, MD; Mutsuo Harada, PhD; Toyoshi Isse, PhD; Toshihiro Kawamoto, PhD; Huizhi Fan, PhD; Pengyuan Yang, PhD; Hiroshi Akazawa, PhD; Toshio Nagai, MD; Hiroyuki Takano, MD; Peipei Ping, PhD; Issei Komuro, MD, PhD; Junbo Ge, MD

Background—Increasing evidence suggests a critical role for mitochondrial aldehyde dehydrogenase 2 (ALDH2) in protection against cardiac injuries; however, the downstream cytosolic actions of this enzyme are largely undefined.

Methods and Results—Proteomic analysis identified a significant downregulation of mitochondrial ALDH2 in the heart of a rat heart failure model after myocardial infarction. The mechanistic insights underlying ALDH2 action were elucidated using murine models overexpressing ALDH2 or its mutant or with the ablation of the *ALDH2* gene (*ALDH2* knockout) and neonatal cardiomyocytes undergoing altered expression and activity of ALDH2. Left ventricle dilation and dysfunction and cardiomyocyte death after myocardial infarction were exacerbated in *ALDH2*-knockout or ALDH2 mutant-overexpressing mice but were significantly attenuated in ALDH2-overexpressing mice. Using an anoxia model of cardiomyocytes with deficiency in ALDH2 activities, we observed prominent cardiomyocyte apoptosis and increased accumulation of the reactive aldehyde 4-hydroxy-2-nonenal (4-HNE). We subsequently examined the impacts of mitochondrial ALDH2 and 4-HNE on the relevant cytosolic protective pathways. Our data documented 4-HNE-stimulated p53 upregulation via the phosphorylation of JNK, accompanying increased cardiomyocyte apoptosis that was attenuated by inhibition of p53. Importantly, elevation of 4-HNE also triggered a reduction of the cytosolic HSP70, further corroborating cytosolic action of the 4-HNE instigated by downregulation of mitochondrial ALDH2.

Conclusions—Downregulation of ALDH2 in the mitochondria induced an elevation of 4-HNE, leading to cardiomyocyte apoptosis by subsequent inhibition of HSP70, phosphorylation of JNK, and activation of p53. This chain of molecular events took place in both the mitochondria and the cytosol, contributing to the mechanism underlying heart failure. (***J Am Heart Assoc.* 2014;3:e000779 doi: 10.1161/JAHA.113.000779**)

Key Words: ALDH2 • apoptosis • heart failure • myocardial infarction • p53

Heart failure (HF), the end-stage of various heart diseases, is a leading cause of mortality in many countries.[1] The underlying mechanisms responsible for the development of HF have not been fully understood, and thus the treatment for HF has yet to improve. HF is a complex syndrome characterized by mechanical dysfunction of the myocardium, defects in bioenergetics, increased cardiac pre- and/or after-load, maladjusted myocardial angiogenesis, altered signal transduction pathways, and abnormal calcium homeostasis; in addition, neurohormonal and inflammatory

From the Shanghai Institute of Cardiovascular Diseases, Zhongshan Hospital and Institutes of Biomedical Sciences (A.S., Y.Z., D.X., H.G., S.W., P.Z., Y.C., J.G.) and Department of Chemistry and Proteome Research Center, Institutes of Biomedical Sciences (H.F., P.Y.), Fudan University, Shanghai, China; Department of Cardiovascular Science and Medicine, Chiba University Graduate School of Medicine, Chiba, Japan (P.W., Y.Q., M.H., T.N., H.T.); Department of Environmental Health, School of Medicine, University of Occupational and Environmental Health, Fukuoka, Japan (T.I., T.K.); Department of Cardiovascular Medicine, University of Tokyo Graduate School of Medicine, Tokyo, Japan (H.A., I.K.); Division of Cardiology, Departments of Physiology and Medicine, David Geffen School of Medicine at UCLA, Los Angeles, CA (P.P.).

*Dr Sun, Dr Zou, Dr Wang, Dr Xu, and Dr Gong contributed equally to this work.

Correspondence to: Junbo Ge, MD, Yunzeng Zou, MD, PhD, or Aijun Sun, PhD, Shanghai Institute of Cardiovascular Diseases, Zhongshan Hospital, Fudan University, 180 Feng Lin Road, Shanghai 200032, China. E-mails: jbge@zs-hospital.sh.cn, zou.yunzeng@zs-hospital.sh.cn, sun.aijun@zs-hospital.sh.cn; Issei Komuro, MD, PhD, Department of Cardiovascular Medicine, University of Tokyo Graduate School of Medicine, Tokyo 113-8655, Japan. E-mail: komuro_tky2000@yahoo.co.jp

Received May 5, 2014; accepted July 11, 2014.

disorders might contribute to all of the pathogenic mechanisms of HF.[2] Moreover, the "mismatch" between the increasing energy demand of cardiomyocytes and the proliferation of mitochondria in cases of cardiac hypertrophy might promote HF development.[3,4] A majority of intracellular reactive oxygen species (ROS) are byproducts of mitochondrial metabolism, and bioenergetic activity and mitochondrial dysfunctions were shown to result in the generation of excess amounts of oxidant stress[5–8] and could further enhance cardiomyocytes apoptosis, which serves as another mechanism for the aggravation of HF.[9–11]

In a separate experiment, we found that the expression levels of 9 protein spots on gels were decreased and other 6 protein spots on gels were increased in rat heart mitochondrial proteins 4 weeks after myocardial infarction (MI) compared with a sham group using 2-dimensional (2D) electrophoresis. In addition, 1 of the decreased spots was identified as aldehyde dehydrogenase 2 (ALDH2) by a mass spectrometry and database comparison (Figure 1A through 1C; Table 1). The phenomena were confirmed in rat (Figure 1D and 1E) and mouse (Figure 2A and 2B) HF models as well as in the failing human heart (Figure 2C and 2D), stimulating our interest in exploring the role of ALDH2 in the development of HF. ALDH2 was reported to serve as a nitrate reductase that specifically catalyzes nitroglycerin and produces nitric oxide.[12,13] Chronic nitrate treatment-induced inhibition of ALDH2 is one of the reasons for nitrate tolerance.[14,15] Several lines of evidence suggest that ALDH2 could act on detoxification of acetaldehyde such as 4-hydroxy 2-nonenol (4-HNE)[16] and may be a key enzyme involved in protection against various cardiac injuries such as ischemia and ethanol toxicities.[17,18]

Table 1. List of Proteins Identified by Proteomics

1. Proteins with more than 5 fold-decrease of expression in failing heart
Mitochondrial proteins
Similar to RIKEN cDNA 1700025B16 (*Rattus norvegicus*)
Aconitase 2 (*Rattus norvegicus*)
Aldehyde dehydrogenase 2, mitochondrial (*Rattus norvegicus*)
LRRGT00108 (*Rattus norvegicus*)
Electron-transfer-flavoprotein, beta polypeptide (*Rattus norvegicus*)
Hypothetical LOC361596 (*Rattus norvegicus*)
RIKEN cDNA 2900053E13 (Mouse)
Other proteins
Myosin, light polypeptide 3 (*Rattus norvegicus*)
Predicted: similar to ribosomal protein L21 (*Rattus norvegicus*)
2. Proteins with more than 5-fold increase in expression in failing heart
Mitochondrial proteins
Dihydrolipoamide S-acetyltransferase (*Rattus norvegicus*)
RIKEN cDNA 2900053E13 (Mouse)
Other proteins
Vimentin (*Rattus norvegicus*)
Tubulin, beta 5 (*Rattus norvegicus*)
Ribosomal protein L8 (*Homo sapiens*)
Protein disulfide-isomerase A6 precursor (*Rattus norvegicus*)

Although the precise mechanisms of downregulation of ALDH2 during the development of HF remain unclear, it has been shown that treatment with a PKC activator upregulated ALDH2 activity and reduced infarct size, and PKC inhibition abolished ethanol-induced increases in ALDH2 activity and cardiac protection against ischemia, suggesting that PKC might be a regulator for ALDH2.[17] In addition, our recent results showed that miR-34a was highly increased, whereas ALDH2 expression was decreased after MI in mice. Overexpression of miR-34a in neonatal rat cardiomyocyte could significantly enhance apoptosis and downregulate ALDH2 expression. Luciferase reporter assay results demonstrated that ALDH2 was a direct target of miR-34a.[19] Taken together, PKC and miR-34a might be responsible for the downregulation of ALDH2.

Although ALDH2/4-HNE have been reportedly involved in protection against various cardiac injuries, the downstream molecular actions of ALDH2/4-NHE are largely undefined. It remains unknown whether the mobilization of mitochondrial ALDH2 affects events in the cytosol and whether cardiac protection results from integrated actions from both mitochondrial and cytosolic locations. Accordingly, using a murine HF model induced by MI, we explored the potential role of ALDH2 in the development of HF and tried to clarify the related molecular chain from mitochondria to cytosol.

Methods

Animals and Gene Manipulation

Adult male Sprague–Dawley rats (200 to 250 g) and wild type (WT) C57BL/6 mice (20 to 25 g) were purchased from Shanghai Animal Administration Center. *ALDH2*-knockout (*ALDH2*-KO) mice were generated, as described previously.[20] Adenoviral vectors encoding *ALDH2* or empty vector were injected into the left ventricular (LV) cavity through the apex of the heart.[21,22] In brief, adenoviral vectors encoding *ALDH2*, dominant negative forms of *ALDH2* (*dnALDH2*), or empty vector (10^9 pfu in 100 μL medium) were injected into the LV cavity through the apex of the heart under temporary clamping of the ascending aorta and pulmonary artery for 40 seconds 2 days prior to the MI procedure.[21] Efficacy of adenoviral vector

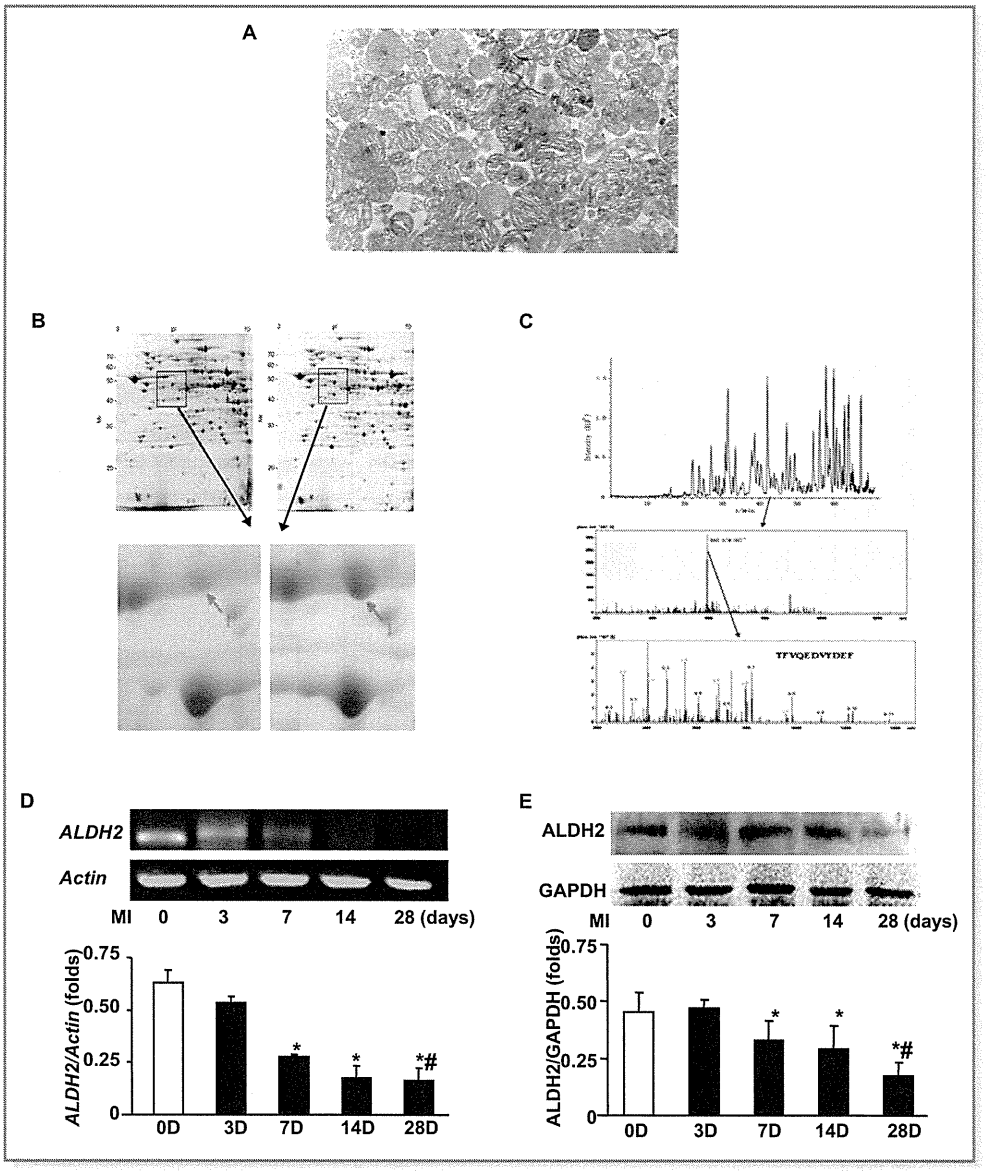

Figure 1. Cardiac mitochondrial proteome and identification of ALDH2 downregulation after MI. Mitochondrial fractions were isolated from the left ventricless of rat hearts at 4 weeks after MI or sham operation. A, Purity of isolated cardiac mitochondria evaluated by electronic microscopy. Mitochondrial fractions were isolated by a method of grade centrifugation, and the purity was 90% to 95%, evaluated by observation under an electronic microscope. B, A subfractional proteomic analysis for cardiac mitochondria. Mitochondria proteins were subjected to a 2D electrophoresis. Representative photographs are shown. Left, MI heart; Right, sham heart. C, Selection of significantly changed spots and identification by the LTQ-ESI-MS/MS. Two-dimensional electrophoresis displayed 15 protein spots that differed significantly in intensity between MI and sham hearts among ≈100 spots. The expression levels of 9 spots decreased and another 6 spots increased in MI rats compared with sham-operated rats. One of the decreased spots was identified as ALDH2. D, Confirmation of expression of *ALDH2* by RT-PCR. Rats were subjected to MI or sham operation for the indicated times. Representative photographs of RT-PCR are shown. β-Actin was used as a loading control. E, Confirmation by Western blot analyses for the expression of cardiac mitochondrial ALDH2. Rats were subjected to MI or sham operation for the indicated time. Representative photographs are shown. GAPDH was used as a loading control. ALDH2 expression was quantified as folds of β-actin or GAPDH. Data are shown as mean±SE from 9 samples. *P<0.05 vs sham; #P<0.05 vs 7 days. ALDH2 indicates aldehyde dehydrogenase 2; D, days; LTQ-ESI-MS/MS, liquid chromatography electrospray ionisation tandem mass spectrometry; MI, myocardial infarction; RT-PCR, reverse transcription–polymerase chain reaction.

transfection into myocardium evaluated by X-gal staining of the LacZ vector was >50% (data not shown).[22] Small interfering RNA (siRNA) or nontargeting control (Sigma-Aldrich) was administered to mice via intraperitoneal injection.[23,24] Briefly, the siRNA of p53 or nontargeting control (Sigma-Aldrich) was administered to mice 2 days before MI via an intraperitoneal injection. Mice received 1.5 μg of siRNA per gram of body weight. Before administration, siRNA was bound to siPORT amine transfection reagent (Ambion) according to the manufacturer's instructions: siPORT amine was incubated for 30 minutes at 22°C in saline. The siPORT amine/saline mixture was then

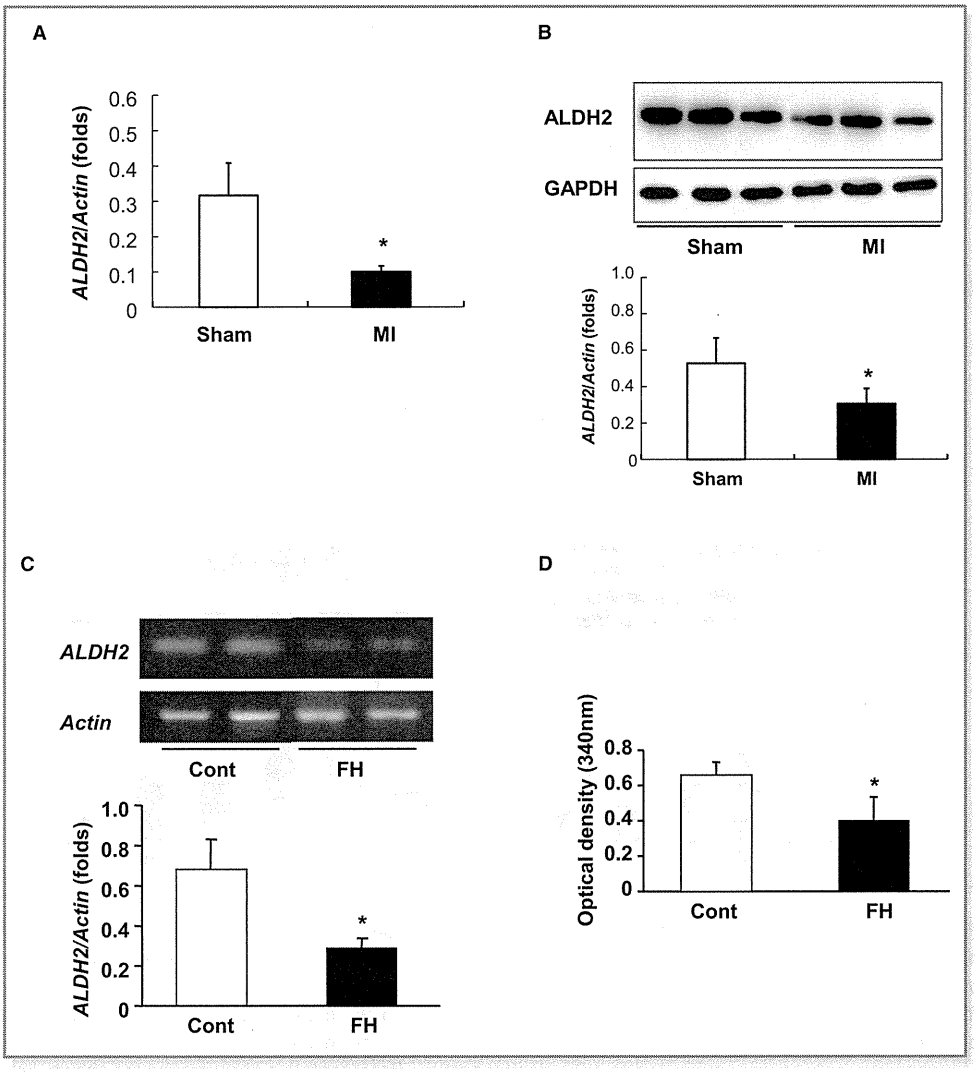

Figure 2. Downregulation of cardiac mitochondrial ALDH2 in mice after MI. Mice were subjected to MI or sham operation for 4 weeks. mRNA or mitochondria protein was prepared from hearts and subjected respectively to RT-PCR (A) and Western blot (B) analyses for ALDH2 expression. Representative photograph of Western blotting is shown. β-Actin or GAPDH was used as a loading control. ALDH2 expression was quantified as folds of β-actin or GAPDH. Data are shown as mean±SE from 9 samples. *P<0.05 vs sham. Expression of *ALDH2* (C) and ALDH2 activities (D) in human hearts. mRNA or mitochondria protein was prepared from 3 controls (aged 30 to 45 years) and 3 failing human hearts (aged 35 to 43 years). A representative photograph of RT-PCR analysis is shown. β-Actin was used as a loading control. *ALDH2* expression was quantified as folds of β-Actin, and ALDH2 activities were expressed as the initial rate of NADH production at 340 nm. Data are shown as mean±SE from 3 hearts. *P<0.05 vs control. ALDH2 indicates aldehyde dehydrogenase 2; MI, myocardial infarction; RT-PCR, reverse transcription–polymerase chain reaction.